Global Solution Properties of Poly(*N*-vinylimidazole) in Ethanol. Macromolecules and Aggregates

G. Savin,[†] W. Burchard,*[,†] C. Luca,[‡] and C. Beldie[§]

Institute of Macromolecular Chemistry, "Albert-Ludwig" University of Freiburg, 79104 Freiburg, Germany, and "Petru Poni" Institute of Macromolecular Chemistry, Romanian Academy of Science, and Department of Physical Chemistry, "Al. I. Cuza" University of Iasi, 6600 Iasi, Romania

Received September 12, 2003; Revised Manuscript Received March 25, 2004

ABSTRACT: Poly(*N*-vinylimidazole) is a weakly basic linear polymer and is soluble in aqueous media and in various alcohols. The present study deals with the global solution properties in absolute ethanol (M_w, R_g, R_h, A_2, and [η]). Samples were prepared by precipitating free radical polymerization in toluene or benzene. Common flexible chain behavior of single macromolecules was found for samples of molar mass $M_w < 8 \times 10^5$ g/mol. However, large aggregates were obtained when longer chains were prepared by reducing the initiator/monomer ratio in the system. At about the same molar mass a 3-fold larger radius was found which only weakly further increased with the corresponding molar mass of the aggregates. Similar breaks in behavior at the same point were found for the hydrodynamic radius, the second virial coefficient, and the intrinsic viscosity. Power law behavior was obtained in both regimes but with different exponents before and after the break point. In the low M_w regime of molecularly dissolved chains the common scaling laws among the various exponents are approximately fulfilled. Above the break point the observed exponents strongly violated these scaling relationships, which indicated the aggregates as not self-similar to each other. This conclusion was confirmed by the behavior of the $\rho = R_g/R_h$ parameter and the apparent segment density and is supported by the decrease of the second virial coefficient and the intrinsic viscosity compared to those of the molecularly dispersed molecules. The apparent density exhibited the expected decrease with M_w for the molecules below the break point, but conversely, it increased for the aggregates and indicated an increasingly more dense packing of segments. The findings awoke the need of considering the *dissolution* mechanism that led to metastable aggregates, rather than the formation of associates under thermodynamic equilibrium conditions.

Introduction

Poly(*N*-vinylimidazole) (PVI) is a synthetic polymer with a fairly simple structure which is presented by Scheme 1. It belongs to the group of vinyl polymers with a heterocyclic ring in the side chain, but in contrast to polystyrene it is water soluble. The structure resembles poly(4-vinylpyridine) with the difference that the pyridine group ($pK_b^{pyridine} = 8.75$) is replaced by a stronger basic functionality of the imidazole group ($pK_b^{imidazole} = 7.05$).

Due to the tertiary amine group, PVI behaves as a weak polybase when strong acids are added. The reaction of this polymer with acidic titrants has been the subject of many studies performed by potentiometry, conductometry, viscometry, ^{1}H NMR, and calorimetry.[1−5] Most of the findings are similar to those observed for poly(vinylpyridine) (PVP). However, there were some particularities with PVI which deserve to be pointed out, because they raise questions which so far have not been fully answered.

Light scattering experiments performed at different protonation degrees in aqueous salt solutions showed a decrease of the molar mass with protonation.[6] The authors suggested intermolecular associations of neutral polymers in aqueous solutions.

Various salts displayed different effects on the neutralization process of PVI.[6] In sodium chloride solutions, the viscosity increased continuously similar to that of polyacids in salt solutions. With sodium bromide or sodium nitrate, the reduced specific viscosity passed through a minimum before starting to increase. This initial viscosity decrease was explained by intramolecular association, thus causing polymer coil contraction.

Scheme 1. Chemical Structure of Poly(*N*-vinylimidazole) and of Its Monomer

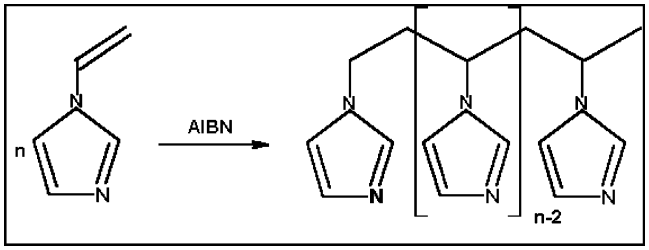

The influence of supporting anions on the acid dissociation equilibria of the conjugated acid of PVI was investigated by potentiometric and calorimetric titrations at various concentrations of NaCl and $NaNO_3$.[4,5] Contact ion pair formation of the anion with the positively charged imidazole group was observed. The effect of NO_3^- ions was found to be smaller than that of Cl^-. The ^{35}Cl NMR study showed that the halogen ion can be bound to the positively charged $PVIH^+$ molecules as well to the neutral polymer. Since no interaction of Cl^- with imidazole (the monomeric ligand) was found, the authors concluded that the polymer skeleton is essentially responsible for the specific interaction between anions and PVI.

Conformational changes of PVI in water but also in methanol were observed. These were explained by

* To whom correspondence should be addressed. E-mail: walther.burchard@makro.uni-freiburg.de.
[†] "Albert-Ludwig" University of Freiburg.
[‡] Romanian Academy of Science.
[§] "Al. I. Cuza" University of Iasi.

10.1021/ma035362g CCC: $27.50
Published on Web 07/20/2004

intrachain hydrogen bonds between protonated and unprotonated imidazole rings.[3,7]

Practical implications of PVI were also studied. These were stimulated by the dual character of the polymer, i.e., the hydrophobic backbone and the hydrophilic functionality of the imidazole ring. Because of this structure, the polymer was able to interact with various other substances, via hydrogen bonds, hydrophobic forces, or Coulombic interactions.

Of scientific interest and great practical importance is the easy complex formation of PVI with a number of different metal ions (Ag^+, Cu^{2+}, Zn^{2+}, Pb^{2+}, Cd^{2+}, Co^{2+})[7,8−14] as well as complexation of PVI with other proton-donating polymers.[15,16] A selective catalytic action of PVI in esterolysis reactions was reported and explained through the formation of a catalyst−substrate complex.[17] Cooperative interaction of imidazole with carboxylic groups was found and used in a template polymerization of 1-vinylimidazole along poly(methacrylic acid) (PMA) chains.[18]

Adsorption of PVI from dilute solutions on silica- and gold-covered substrates was demonstrated by reflectometry.[19] Depending on the pH value and the substrate, the polymer adsorption was determined by different forces. At pH 10, the neutral macromolecules were bound to the silica wafer through H-bonds, whereas on gold surfaces, coordinated binding was suggested.

PVI was also found to be an effective polymeric anticorrosion agent for copper at elevated temperatures[20,21] and to act as a compatibilizer for polyethylene/polystyrene blends.[22]

This lengthy list of often not well explained particularities makes clear that a detailed characterization of the polymer in solution may be of help for a better understanding of this material and for future application. In the beginning the study was considered as a routine work, but in the course of characterization it disclosed an unexpected complexity, which probably originated from the history of polymer synthesis.

Prior to us, PVI was characterized by the group of Tan.[3,6,22] Samples were prepared by precipitation free radical polymerization in a molar mass range smaller than $M_w = 10^6$ g/mol. The samples were investigated with regard to the following aspects: (i) solubility behavior in water and methanol in the presence of an electrolyte, (ii) chain dimensions and flexibility, (iii) effect of solvent polarity and neutral electrolytes on the chain conformations.

The study of molar masses larger than $M_w = 10^6$ g/mol was avoided, probably because of difficulties in estimating the true molar mass and true radius of gyration in that region. When we investigated the samples in a high molar mass region of $M_w > 10^6$ g/mol, the properties gave evidence of metastable aggregates. The purpose of the present study is to unravel the occurring aggregate structures and to elucidate the architecture of the high molar mass PVI samples besides the molecularly dissolved macromolecules.

Our findings will be reported in two series of three papers each. The first series deals with the properties in absolute ethanol, and the second one will be concerned with the solution properties in various alcohols and at different temperatures, in aqueous salt solutions, and finally in aqueous hydrocloric and acetic acids of different molarities. In the present paper the global structure of PVI molecules and aggregates in ethanol is described in a region up to several million grams per mole in molar mass. To avoid confusion in the following outline, we have to make a comment on nomenclature. The symbol M_w stands for the *molar mass* of molecules as well as of aggregates. Such a molar mass can present a *molecular weight* or a *particle weight*, but whenever possible, we avoid the older definition and speak of molar masses of macromolecules or of aggregates. Static and dynamic light scattering and viscometry were applied. A detailed characterization of the aggregates by static light scattering has already been given.[23] The third paper in this series will deal with the dynamic properties of PVI in ethanol.

Experimental Section

Materials. Benzene (thiophene-free) from Aldrich was purified by distillation over sodium, prior to use. 1-Vinylimidazole (VI) (Aldrich) was vacuum-distilled at 76 °C/18 mmHg, before polymerization. α,α′-Azobisisobutyronitrile (AIBN) was purified by recrystallization from methanol at 30 °C. The other materials were reagent grade chemicals, used as received.

Polymerization. Three poly(*N*-vinylimidazole) samples (PVI1, PVI2, PVI3) were synthesized in the laboratory of the "Petru Poni" Institute of Macromolecular Chemistry, Iasi, Romania, according to the literature[24,25] using toluene as the precipitating solvent. The other samples of poly(*N*-vinylimidazole) were obtained in the present laboratory by precipitation free radical polymerization in thiophene-free benzene with AIBN as the initiator. Temperatures in the range of 60−70 °C were applied. The polymerization was performed under deoxygenated conditions (argon and vacuum). The gritty precipitated polymer was collected by filtration and dried in a vacuum oven at 35 °C for several days. Some of the samples were purified by reprecipitation using different solvent/precipitant pairs. The materials thus obtained were freeze-dried from an aqueous solution and stored in an exsiccator at room temperature. The polymers used in this study are listed in Table 1, which also gives details of the polymerization conditions and the solvent/precipitant components.

Polymer samples of different molar masses were obtained by varying the monomer-to-initiator ratio in the reaction vessel and by changing the monomer concentration in benzene. In one case a series of eight fractions was prepared from PVI1 by precipitating fractionation.

Polymer Fractionation. Fractions of different molar masses were prepared from sample PVI1 by stepwise precipitation of a 1-butanol solution with *n*-hexane. The fractions were dissolved in deionized water (ultrapure water system, Milli-Q, 18.2 MΩ cm), freeze-dried, and stored in an exsiccator.

Static Light Scattering (SLS). SLS measurements were performed with a computerized and modified SOFICA photogoniometer (G. Baur, Instrumentenbau, Hausen, Germany), equipped with a He−Ne laser ($\lambda_0 = 632.8$ nm). Measurements were made in an angular region from 30° to 145°, in steps of 5° in absolute ethanol. Freshly distilled and 0.2 μm pore size filtered toluene was used to calibrate the instrument. The values for the refractive index increments dn/dc were measured with a Brice-Phoenix differential refractometer, at 20 °C and $\lambda_0 = 632.8$ nm. A xenon lamp served as a light source, and the required wavelength was selected by a monochromator. A value of dn/dc = 0.165 mL/g was found in ethanol. All measurements

Table 1. Details of Poly(*N*-vinylimidazole) Free Radical Polymerization under Precipitating Conditions[a]

	no.	sample	[I]/[M], no solv	solv	[M]/[solv]	[I]/[M] in soln	*T*, °C	*t*, h	M_w, 10^{-5} g/mol
I	1	PVI1	0.005	Benz	0.15	0.0333	60	48.0	5.37
	2	PVI2	0.0075	Benz	0.15	0.0500	60	48.0	2.20
	3	PVI3	0.019	Benz	0.15	0.0667	60	48.0	1.60
II	4	PVIm1	0.010	Tol	0.70	0.143	65	1.5	1.95
	5	PVIm2	0.010	Tol	1.00	0.010	70	35.0	1.10
	6	PVIm3	0.002	Tol	1.00	0.002	70	11.0	36.60
III	7	PVID	0.001	Benz	0.20	0.005	70	3.0	26.90
	8	PVIC	0.002	Benz	0.40	0.005	70	3.0	103.00
	9	PVID	0.001	Benz	0.60	0.00167	70	24.0	586.00
	10	PVIA[b]	0.001	Benz	0.80	0.00125	70	24.0	7.93[b]
IV	11	PVI I	0.005	Benz	0.14	0.0357	60	6.0	2,57

[a] The different groups of preparation are indicated by Roman numerals. Mostly the notation of column 2 is used in the text. [I]/[M] is the mole ratio of the initiator (AIBN) to the monomer. Due to the added solvent the monomer concentration is diluted and is given in column 6. This ratio of moles determines the chain length at a given temperature. An increase of the reaction temperature causes a drastic decrease of the chain length, mainly due to the larger production of radicals, which increases the rate of termination. The solvents benzene (Benz) and toluene (Tol) are precipitants for the polymer. Samples 6−10 represent the conditions under which aggregates were obtained. [b] Sample PVA formed a swollen gel in ethanol. After ultracentrifugation a soluble sol fraction was found in the supernatant; the molar mass of this aggregate refers to this sol fraction.

were carried out at 20 °C. The range of the studied polymer concentrations was between 0.1 and 10 mg/mL. Prior to the measurements, all solutions of *molecularly dispersed* samples were repeatedly filtered through 0.45 μm Millipore membrane filters in a laminar flow cabinet. Filtration of the PVI aggregates through these narrow pore size filters was not possible. We tested pore sizes of larger dimensions and found only with the 5 μm pore size filters no inhibition on filtering. All scattering cells were made dust-free by rinsing them with freshly distilled acetone in a special fountain-like apparatus (Dinkelavker, Mainz, Germany).

Dynamic Light Scattering (DLS). For all solutions DLS measurements were carried out with the same samples as used for static LS. An ALV photogoniometer (ALV-Langen, Hessen, Germany) was used, equipped with an ALV 5000 correlator. A krypton ion laser (Spectra Physics 2002) operating at 647.1 nm wavelength was used as the light source. Measurements were made at 20 °C in an angular range from 40° to 140°, in steps of 10° or 15°.

Theory

Static Light Scattering.[26] The excess reduced scattering intensity $R_\theta = i(\theta)r^2/I_0$ (Rayleigh ratio) was determined as a function of the scattering angle θ and polymer mass concentration c, with $i(\theta)$ the scattering intensity and I_0 the vertically polarized primary beam intensity.

The data were analyzed by the Zimm procedure and modifications according to Berry and the Guinier approximation, using the Debye equation

$$\frac{Kc}{R_\theta} = \frac{1}{M_w P_z(q)} + 2A_2c + \dots \quad (1)$$

in which

$$K = \frac{16\pi^2}{N_A\lambda_0^4}\left(n_0\frac{dn}{dc}\right)^2 \quad (2)$$

is the contrast factor with dn/dc the refractive index increment. $P_z(q)$ is the particle scattering factor, M_w the weight-average molar mass, and A_2 the second osmotic virial coefficient. The subscript z denotes the z-average. The particle scattering factor $P_z(q)$ is given by the ratio

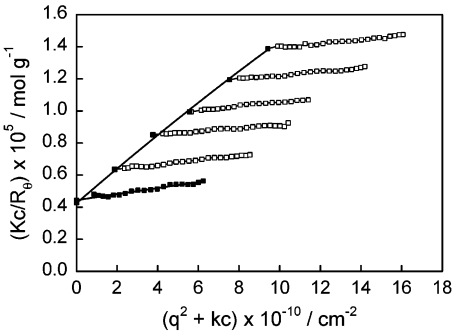

Figure 1. Zimm plot from PVI2 in ethanol for concentration from 2 up to 10 g/L. $M_w = 2.2 \times 10^5$ g/mol, $A_2 = 4.64 \times 10^{-4}$ mol mL g^{-2}, and $R_g = 33$ nm. For the sake of clarity the lines through the various scattering angles are not shown.

$P_z(\theta) = R_\theta/R_{\theta=0}$ and is for small values of qR_g represented by

$$\frac{1}{P_z(q)} = 1 + \frac{1}{3}q^2{R_g}^2 \quad (3)$$

where $R_g^2 = \langle S^2\rangle_z$ is the z-average mean-square radius of gyration and q is the magnitude of the scattering vector and is given by the equation

$$q = \left(\frac{4\pi n_0}{\lambda_0}\right)\sin\left(\frac{\theta}{2}\right) \quad (4)$$

Note that both quantities $P_z(\theta)$ and $qR_g \equiv u$ are dimensionless and establish a universal, molar mass independent curve if self-similarity is obeyed..

Equation 2 requires a double-extrapolation procedure. If the angular dependence is extrapolated to $q = 0$, the concentration dependence of the reciprocal apparent molar mass is obtained:

$$\frac{1}{M_{app}(c)} = \frac{1}{M_w} + 2A_2c + 3A_3c^2 + \dots \quad (5)$$

The actual molar mass is obtained by extrapolation of $1/M_{app}(c)$ to zero concentration. The required double extrapolation can be made in a Zimm plot[27] where Kc/R_θ is plotted against $q^2 + kc$. Mostly a group of parallel lines is obtained. An example is shown in Figure 1.

Linear dependence is obtained for common flexible linear chain molecules.[27] In some cases, however, the

angular dependence displays a curvature. If this curvature exhibits an upturn, large globular particles are indicated which are recognized as aggregates. Such an upturn is observed with latex particles and monodisperse branched or spherelike structures, e.g., dendrimers.[28] Stiff chain behavior, on the other hand, causes a downturn toward the q^2 axis. However, such concave behavior can also be created by a large polydispersity, for instance, when two components of very different molar masses are present. In such cases a special curve analysis is required to separate both components. The technique has been described in detail in a previous paper.[23]

The convex curvature can cause misleading results when the experimental data are extrapolated to $q^2 = 0$, and even negative molar masses could be obtained. In any case the linear initial part determines the mean square radius of gyration, and for this reason a suitable plot is desirable which gives a linearization over a longer q^2 range. For compact spheres the upturn in the Zimm representation is transformed into a linear dependence when $\ln(Kc/R_\theta)$ is plotted against q^2 (Guinier plot),[29] but also for branched structures the convex curvature in the Zimm presentation becomes largely linearized in such a Guinier plot. In this case the initial part of the particle scattering factor is given by Guninier's approximation[29]

$$P_z(q) = \exp\left(-\frac{1}{3}R_g{}^2q^2\right) \tag{6}$$

and the scattering curve at zero concentration then is represented by

$$\ln\left(\frac{Kc}{R_\theta}\right) = \ln\left(\frac{1}{M_w}\right) + \frac{1}{3}q^2R_g{}^2 \tag{7}$$

Even for scattering curves which show a downturn, the Guinier plot often gives a well-developed linear initial part (which determines the mean square radius of gyration). The slope can be found by special fit procedures. Problems in accuracy have to be kept in mind. In some cases the whole angular dependence could be well fitted by a polynomial of the fourth or fifth order in q^2, in which the first coefficient of the q^2 term is $a_1 = R_g{}^2/3$.

Despite apparently very satisfying fits, the initial coefficient may be fairly inaccurate. More reliable results are obtained when only the initial part (the first points in the q^2 dependence) is used and a quadratic fit is applied. These two procedures give good approximations for the radius of gyration. Larger errors are to be expected for the intercept that gives $\ln(1/M_w)$. Here errors on the order of about 20% cannot be avoided. Notably, the Guinier plot presents the advantage that the determination of molar mass and radius of gyration is decoupled, which is not the case when a Zimm plot is used. This fact is particularly advantageous for particles of very large molar mass. In this case the intercept in a Zimm plot is very close to zero. This causes an immense error, and sometimes leads to a negative molar mass. Such a meaningless result can never be obtained in the logarithmic Guinier presentation. After the serial fit of the angular dependence from each concentration and fits of the concentration dependence of the data from each scattering angle, a final procedure called a "smooth" fit is employed in which the whole set of data are used for a simultaneous fit.

Dynamic Light Scattering. In addition to static light scattering, the PVI properties were investigated by dynamic light scattering. In the dynamic light scattering experiment a normalized intensity−time correlation function (TCF), $g_2(t,q)$, is measured:[30]

$$g_2(t,q) \equiv \frac{\langle i(0,q)\, i(t,q)\rangle}{\langle i(0,q)\rangle^2} \tag{8}$$

where $i(t,q)$ is the scattering intensity at a certain delay time from a reference time $t = 0$. In dilute solutions $g_2(t,q)$ can be expressed in terms of the normalized field TCF $g_1(t,q)$ using the Siegert relationship

$$g_2(t,q) = 1 + \beta|g_1(t,q)|^2 \tag{9}$$

with a coefficient $\beta < 1$ that depends on the quality of coherence. Unimodal fiber optics were used in the present study for which the β-value was 0.98, close to the theoretical value of 1. For short delay times $g_1(t,q)$ is well approximated by a single-exponential decay:

$$g_1(t,q) \approx \exp(-\Gamma(q)t) \quad \text{if} \quad \Gamma(q)t < 1 \tag{10}$$

This decay time is related to an apparent mutual diffusion coefficient as[27,30]

$$\Gamma(q) = q^2D_{app}(q,c) \tag{11}$$

where

$$D_{app}(q,c) = D_z(1 + k_Dc)(1 + CR_g{}^2q^2 - ...) \tag{12}$$

D_z is the translation diffusion coefficient of the particle's center of mass, where the subscript indicates the z-average over the molar mass distribution. The first set of parentheses on the right-hand side in eq 12 describes the concentration dependence, which often is well represented by a linear dependence:

$$D_{app}(c,q\rightarrow 0) \equiv D_c \approx D_{trans}(1 + k_Dc) \tag{13}$$

with k_D as a coefficient that depends on the second virial coefficient as well as on the concentration dependence of the hydrodynamic friction.

The ratio $\Gamma(q)/q^2 \equiv D_{app}(c,q)$ is often angular dependent and is then only an apparent diffusion coefficient which for small $q^2R_g{}^2 < 2$ is given by eq 12. This angular dependence results from segmental motions and polydispersity.

The double extrapolation of $D_{app}(c,q)$ to $c = 0$ and $q = 0$, which can be done in a dynamic Zimm plot, gives the translation diffusion coefficient from which the hydrodynamic radius is obtained according to the Stokes−Einstein relationship

$$R_h = \frac{kT}{6\pi\eta_0D_z} \tag{14}$$

where k is the Boltzmann constant, T is the absolute temperature of the solution, and η_0 is the solvent viscosity. The angular dependence of $D_{app}(q)$ is pronounced with the aggregates and will be evaluated in a separate paper.

Results

Zimm Plots and Modified Representation of Static Light Scattering Data. In the low molar mass

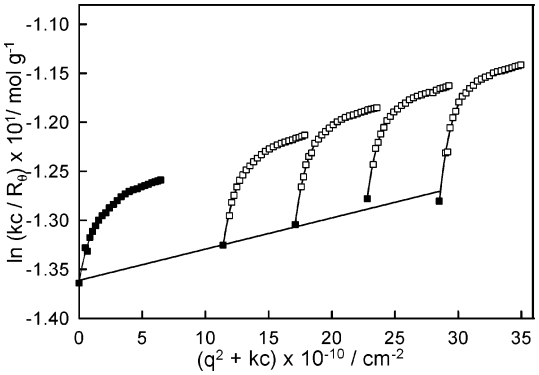

Figure 2. Guinier plot of the data from PVIA in ethanol at 20 °C (c = 4−10 g/L) as shown in Figure 1 but now in the modified Guinier representation. Accurate determination of the molecular parameters became possible. $M_w = 7.93 \times 10^5$ g/mol, $R_g = 150$ nm, and $A_2 = 5.32 \times 10^{-5}$ mol mL g^{-2}.

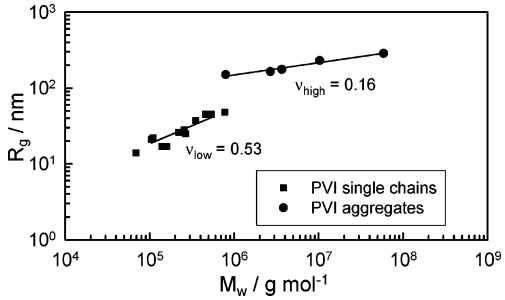

Figure 3. Radii of gyration R_g as a function of molar mass M_w for PVI samples in ethanol, in a double-logarithmic plot. The regression lines follow eq 15. Two different slopes were observed. The steeper curve showed the common increase of the dimensions with the mass for flexible chain molecules. The flatter line refers to aggregates and revealed a strong mass increase by only a small change in the radius of gyration. Note that the sample PVA (near the break point) represents the sol fraction from a physical gel.

region up to $M_w \approx 8 \times 10^5$ g/mol the Zimm plots showed normal behavior of molecularly dissolved chain molecules, as was already shown with one example in Figure 1. However, beyond $M_w \approx 8 \times 10^5$ g/mol the Zimm plots displayed an abnormal feature with a marked downturn in the small-angle scattering regime. No reasonable extrapolation was possible in this common Zimm plot. The corresponding Guinier representation as shown in Figure 2 likewise exhibited marked curvatures, but these curves are approximately parallel to each other, which indicates no change in structure as the concentration is increased. The small-angle part is linear over a wide range and permitted an accurate determination of the radius of gyration of the polydisperse system. Also a reliable weight-average molar mass could be obtained. The high values of the molar mass render these samples as aggregates.

At this point some remarks on the extrapolation procedure may be suitable. As was already mentioned in the Experimental Section the whole process of the measurements is controlled by a computer. Each scattering angle was repeated five times before the step motor moved to the next scattering angle. The data were directly represented on the monitor screen. Sometimes at a special angle strong deviations from the otherwise smooth curve toward much larger scattering intensities occurred. In this case, the cylindrical light scattering cell was slightly rotated and the measurement was repeated. The results were then plotted and evaluated by a special algorithm. First, the raw data from the measurement were represented in a Zimm plot, a Berry plot, and a Guinier plot. Each angular dependence from the various concentrations was fitted by a polynomial (mostly of the second order but sometimes up to the fifth order) to find the value at zero scattering angle. The same procedure was applied to each angle from the various concentrations, which gave the data of the angular dependence at zero concentration. This concentration dependence was mostly fitted by a linear regression but sometimes also with a second-order polynomial. The solid lines in the plots of this paper are always regression lines, and the symbols represent the experimental data. Finally, the quality of the obtained result was checked with an additional routine called a smooth fit in which the whole set of data are used simultaneously. The applied algorithm uses as starting points the data from the first routine and uses a regularization constraint that changes with concentration, and the scattering angle should be continuous and should show no erratic scatter. Finally, the diagrams and the evaluated data for the molar mass, radius of gyration, and second virial coefficient are printed out together with the mean square deviation. Because of the high precision obtained with the scattering data from the aggregated high molar mass PVI samples, the experimental errors were mostly less than 20% for M_w, <5% for R_g, and about 10−20% for A_2. The experimental data (also of the extrapolated curves) but not those of the fitted curves were exported into Origin or Sigma Plot programs for establishing other representations and for special fitting procedures, for instance with a special model. For details see ref 28.

Radius of Gyration. Quite generally, the radius of gyration depends characteristically on the molar mass of the particles.[31] Therefore, a first impression of the shape of the PVI macromolecules could be gained from the experimentally observed particle molar mass dependence of R_g. The experimental data exhibited an unexpected spectacular behavior with a break around a molar mass of $M_w \approx 8 \times 10^6$ g/mol. The sudden jump in the solution properties at an apparently well defined molar mass should not be overvalued. Clearly, as shown in the previous paper,[23] the samples in the high molar mass regime are aggregates. However, it has to be kept in mind that PVIA did not properly dissolve in ethanol like the other samples but formed a swollen gel. The sample PVIA in the following figures corresponds to the sol fraction that was obtained from the supernatant of the ultracentrifuged gel. Unexpectedly, the particle properties fell in line with those of the other aggregates. The double-logarithmic plot of R_g as a function of M_w (Figure 3) gave two straight lines of different slopes. For the molecularly dissolved samples with $M_w < 8 \times 10^5$ g/mol, a steeper curve was obtained than for the aggregates of large molar masses ($M_w > 8 \times 10^5$ g/mol). In this region, the mass increased strongly (by a factor 3) but the corresponding z-averages of the radii of gyration changed their values by no more than 12%.

Power law behavior represented both regimes, given by the general relationship

$$R_g = KM_w^{\nu} \tag{15}$$

For self-similar objects, such as molecularly dissolved linear chains or randomly branched macromolecules, the thermodynamic quality of the solvent could be estimated from the value of the exponent ν, and a preliminary

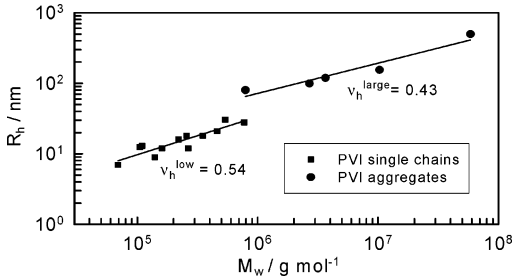

Figure 4. Double-logarithmic plot of the hydrodynamic radius R_h versus the particle molar mass M_w. R_h was calculated from the translational *z*-average diffusion coefficient D_z via eq 14 with $T = 293.16$ K and $\eta = 1.1981$ cP. The slope of the hydrodynamic radius decreases from $\nu_h^{low} = 0.54$ in the low molar mass regime to $\nu_h^{high} = 0.43$ in the high molar mass regime of the aggregates.

suggestion of the molecular shape can be made.[31] From a theoretical point of view, the exponent can vary from $\nu = 0.33$ for hard spheres up to $\nu = 1$ for rigid rods. For single linear chains a value of $\nu = 0.5$ refers to unperturbed Gaussian coil dimensions to be expected in a Θ-solvent, and $\nu = 0.588$[32] indicates good solvent conditions, i.e., large excluded-volume effects and positive second virial coefficients. In the low molar mass region ($M_w < 8 \times 10^5$ g/mol) $\nu = 0.53$ (Figure 3) was obtained in agreement with expectation for molecularly dissolved flexible chains. The value indicated ethanol as a marginally good solvent for linear random coil conformations. For the aggregates with $M_w > 8 \times 10^5$ g/mol a much lower exponent of $\nu = 0.16$ was found. Under the presupposition that the macromolecules have the same structure in both molar mass regimes, this small value could mean a decrease of the solvent quality. However, this interpretation is at variance with the marked increase of R_g around $M_w = 8 \times 10^5$ g/mol. Apparently, a change in the macromolecular architecture has taken place on the basis of aggregation of several polymer chains. This conclusion is confirmed by the behavior of the second virial coefficient and the intrinsic viscosity (see below).

Hydrodynamic Radius. Figure 4 shows the molar mass dependence of the hydrodynamic radius. Similar to Figure 3 the hydrodynamic radii fall into two groups of $M_w < 8 \times 10^5$ g/mol and $M_w > 8 \times 10^5$ g/mol. The exponent in the low molar mass regime ν_h has nearly the same value as R_g (Table 3). However, in the high molar mass regime the deviation is with $\nu_h = 0.43$ significantly larger than that with $\nu = 0.16$.

Second Virial Coefficient. Figure 5 shows the molecular weight dependence of A_2. Again a clear break in behavior occurred around $M_w \approx 10^6$ g/mol. Like the radius of gyration, A_2 displayed power law behavior with respect to M_w:

$$A_2 = K_{A_2} M_w^{-a_{A2}} \qquad (16)$$

Different exponents, below and above the break point (at $M_w \approx 8 \times 10^5$ g/mol), were observed (Figure 5). In the region of low particle mass a small exponent of $a_{A_2} = -0.15$ was found, a value that is characteristic of randomly coiled and molecularly dispersed linear chains in a good solvent. However, the decrease of the second virial coefficient with M_w was faster for the high molar mass PVI samples where an exponent of -0.56 was obtained. This fact requires a more detailed consideration, which is given below.

Table 2. Molecular Parameters of PVI Chain Molecules and Aggregates in Ethanol at 20 °C

sample	M_w, 10^{-6} g/mol	R_g, nm	A_2, 10^4 mol mL g^{-2}	R_h, nm	$[\eta]$, mL/g
Single Chains					
PVI fr VIII	0.069	14	5.47	7	59.1[b]
PVI fr VII	0.140	17	3.19	9	81.7[b]
PVI fr VI	0.265	25	5.50	12	127.4[b]
PVI fr IV	0.350	37	4.07	18	169.0[b]
PVI fr III	0.460	45	3.56	21	198.6[b]
PVI fr I	0.771	48	2.54	28	224.2[b]
PVIm1	0.105	21	1.65	12	30.4
PVIm3	0.110	22	1.69	13	36.8
PVI3	0.160	17	1.67	12	65.1
PVI2	0.220	26	1.63	16	84.5
PVI1	0.538	45	2.31	30	
Aggregates					
PVIA[a]	0.793	150	0.532	80	122.3
PVID	2.69	164	0.226	99	183.2
PVIm2	3.66	176	0.114	119	233.4
PVIC	10.3	230	0.077	155	253.0
PVIB	58.6	285	0.046	497	379.0

[a] Sol fraction from a swollen gel in ethanol. [b] Fractions.

Table 3. Experimental and Theoretical Exponents of Scaling Relationships for the Investigated Systems

sample	ν^{exp}	ν_h^{exp}	$a_{A_2}^{exp}$	$a_{A_2}^{th}$ a	$a_{[\eta]}^{exp}$	$a_{[\eta]}^{th}$ b
low molar mass	0.53	0.54	−0.15	−0.41	0.56	0.59
high molar mass	0.16	0.43	−0.56	−1.52	0.24	−0.52

[a] $a_{A_2}^{th}$ was calculated according to $a_{A_2}^{th} = 3\nu^{exp} - 2$. [b] $a_{[\eta]}^{th}$ was calculated according to $a_{[\eta]}^{exp} = 3\nu^{exp} - 1$.

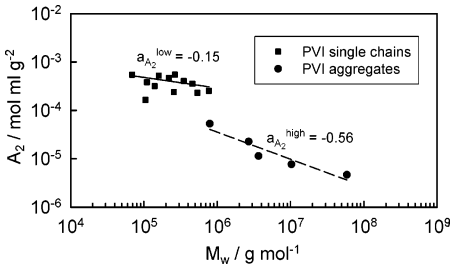

Figure 5. Double-logarithmic plot of the second virial coefficient A_2 versus molar mass M_w. Two different exponents were obtained in regions below and above a break point around $M_w = 8 \times 10^5$ g/mol.

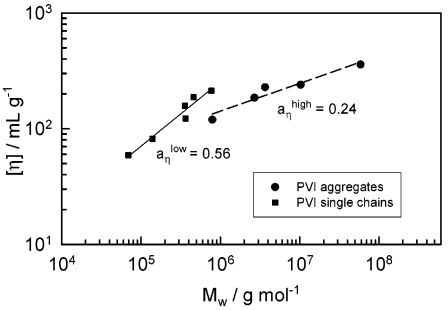

Figure 6. Dependence of the intrinsic viscosity $[\eta]$ on the molar mass. Again, around $M_w = 8 \times 10^5$ g/mol a break and a flatter slope were observed for the higher M_w.

Intrinsic Viscosity. Similar behavior was observed with the intrinsic viscosity as is shown in Figure 6. Both *A_2 and $[\eta]$ decreased* beyond the break point, whereas *R_g and the hydrodynamic radius R_h increased*.

Scaling Behavior. The solvent power and the interaction between two particles in solution are given by the second virial coefficient.[31] The interaction between two different macromolecules is mainly determined by

Table 4. Estimations of Fractal Dimensions d_f, Measured from the Slopes of Two Different Plots, and Comparison with Theoretical Values for Three Structures

Theoretical values $M_w = K R_g^{df}$		Experimental slopes for internal structure of aggregates $\log(R_\theta) = \log K' - d_f \log(q)$	
Linear chains	$d_f = 1.70$-2.00		
Branched chains	$d_f = 2.00 - 2.50$	PVIA***	max. slope = 0.55**
Hard spheres	$d_f = 3.0$	PVID	max. slope = 0.80**
		PVIm2	max. slope = 0.94**
Experimental values for global structure $M_w = K R_g^{df}$		PVIC	slope 1 = 1.63
			slope 2 = 1.17
PVI single chains	$d_f = 1.89$	PVIB	slope 1 = 2.67
PVI aggregates	$d_{f,app*} = 6.25$		slope 2 = 1.66

*This value has no physical meaning and is considered as an apparent fractal dimension.
**Asymptote was not yet reached. ***PVIA is the sol fraction from a gel.

the volume of the particle and is modified by attractive forces and the extent of coil−coil interpenetration.[31] Expressed in mathematical terms one has

$$A_2 = 4\pi^{3/2} N_A \frac{R_g^3}{M^2} \Psi \tag{17}$$

where Ψ is the coil−coil interpenetration function, which for large excluded-volume interaction approaches a constant value which depends on the particle architecture.[28,32]

Power law behavior is often taken as an indication of self-similarity.[32−35] In such cases the exponents from the molar mass dependencies of R_g, A_2, and $[\eta]$ should obey the scaling laws[36]

$$a_{A_2}^{th} = 3\nu - 2 \tag{18}$$

$$a_{[\eta]}^{th} = 3\nu - 1 \tag{19}$$

The theoretical values $a_{A_2}^{th}$ and $a_{[\eta]}^{th}$ derived from ν and the experimental values $a_{A_2}^{exp}$ and $a_{[\eta]}^{exp}$ are compared in Table 3. The aggregates above the break-point clearly violate the scaling conditions. For the low molar mass region the situation is not as clear. Even if one takes into account a fairly high inaccuracy of the A_2 measurements, which causes a variation in the exponent of $a_{A_2}^{exp} = -0.15 \pm 0.07$, the scaling relationship between ν and a_{A_2} is not fulfilled. The reason for this could be that the constant asymptotic value Ψ^* of the interpenetration function was not yet reached. For the viscosity, on the other hand, good agreement was found when eq 19 was applied.

Fractal Dimensions. Commonly, the molar mass dependence of R_g is written in the manner of eq 15. On the other hand, the molar mass can be expressed as a function of the radius of gyration:

$$M_w = K' R_g^{d_f} \tag{20}$$

Evidently, the exponent now defines a mass dimension which for disordered systems no longer is an integer, and therefore is called a fractal dimension, denoted as d_f.[34,35] Thus, the exponent ν is related to a characteristic fractal dimension of self-similar objects by the relationship

$$d_f = 1/\nu \tag{21}$$

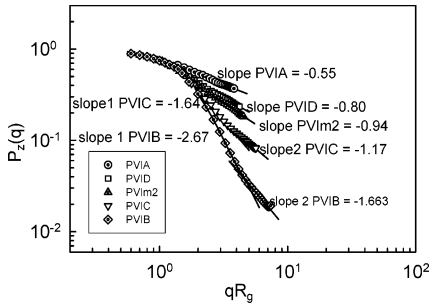

Figure 7. Double-logarithmic plot of particle scattering factors of the PVI aggregates as a function of the normalized scattering vector $u = qR_g$. The asymptotic slopes represent the fractal dimension d_f of substructures in the particle. The intermediate slopes probably display the transition from the global core to dangling chain behavior.

Applying eq 21 to the experimental exponents ν in the two regimes, a fractal dimension of $d_f = 1.89$ is found for the macromolecules in the low molar mass regime (Table 4). This value is common for single coils of linear chains in a marginal solvent. For the aggregates of $M_w > 8 \times 10^5$ g/mol, a value of $d_f = 6.25$ would be obtained. Such a fractal dimension is a physically meaningless result, because in the laboratory three-dimensional world, the mass fractals cannot exceed a value of $d_f = 3.0$. In fact, the scaling relationship of eq 21 no longer is valid if self-similarity is not present.

Often, the fractal dimensions can also be evaluated from the asymptotic angular dependence of the particle structure factor, $P_z(q)$, at large q-values on a double-logarithmic scale. In this kind of examination d_f describes the *internal* structure of the aggregated particles, in contrast to eq 21, which is related to the *global properties of different* particles or macromolecules. In Figure 7 the particle scattering factors of PVI samples are plotted on the double-logarithmic scale against qR_g, and these results are compared with the theoretically derived properties of the soft sphere model[37] (Figure 8). This model represents dendrimers in which a linear spacer of Gaussian behavior is introduced connecting the various branching generations. For the small macromolecules ($M_w < 8 \times 10^5$ g/mol) the required asymptote region of $qR_g > 4$ was not reached, since the experimentally accessible q range was too small. For the highest molar mass PVI particles, power law behavior was observed at large u, sometimes also approximately in the intermediate range, but with very different

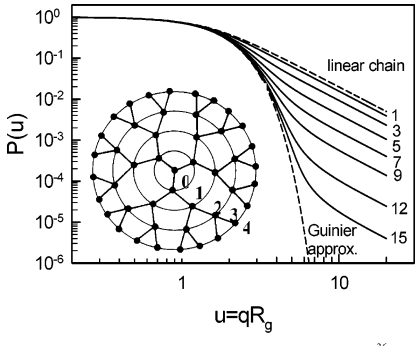

Figure 8. The same plot as in Figure 7 for the soft sphere model[37] of different generations as indicated. The model represents generalized dendrimers in which the various generations are connected via spacers. In the present representation a spacer of DP = 7500 was chosen that corresponds to a PVI molecule shortly below the break point where aggregates were found. Note the similarity in the deviation from the globule behavior.

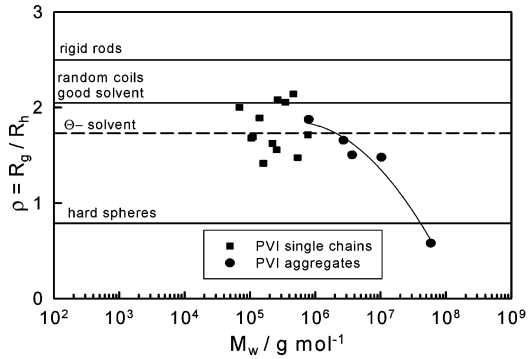

Figure 9. Dependence of the ρ-parameter on the particle mass. The parameter $\rho = R_g/R_h$ showed no molar mass dependence in the low molar mass regime. In the high molar mass regime ρ dropped from a value of 1.87 to 0.58 with increasing molar mass.

Table 5. Experimental ρ-Value for PVI in Ethanol Compared to Theoretical ρ-Values for Some Polymer Architectures

theoretical values		experimental values	
polymer system	ρ-parameter	sample	ρ-parameter
microgel	0.35−0.55	PVI single chains	1.55
hard sphere	0.774	PVIA aggregate	1.87
star molecule	1.10−1.70	PVID aggregate	1.66
random aggregate	1.78	PVIm2 aggregate	1.50
polydispersed coil	1.78	PVIC aggregate	1.48
rigid rod	>2.00	PVIB aggregate	0.58

apparent d_f exponents for the five samples (Table 4). A common power law behavior with the same exponent over the whole molar mass region is expected for "self-similar structures".[33] The slope of about −1, i.e., $d_f \approx 1$, obtained for PVID and PVIm2 would indicate fairly stiff, almost rodlike, linear objects. The larger slopes of about −1.3 for PVIB and −1.2 for PVIC are more in accordance with semiflexible behavior of these particles. In addition the curves of different samples do not establish one unique curve as required for self-similar samples. In any case, the asymptotic slopes (denoted as slope 2 in Figure 7) drastically deviate from the reciprocal value of the exponent ν. Interestingly, the theoretical curves for the soft sphere model of various branching generations (Figure 8) show strikingly similar behavior.[23] The asymptotic slope in this model in all cases is −2, which is exactly the negative fractal dimension of a Gaussian chain. This soft sphere model is presented by a seemingly universal globular behavior and in the region of large q-values, where short distances are probed, by that of short linear chains. The soft sphere model has a heterogeneous structure consisting of a globular core and pending linear chains, and therefore, soft sphere particles of various generations are not self-similar to each other. In a recent paper by Dozier et al.[38] the authors came to a similar conclusion and used this fact for an efficient fit procedure.

Thus, with these checks we came to a first conclusion that despite power law behavior, found for the radius of gyration as a function of the PVI aggregate molar mass, these samples are not objects self-similar to each other. The various asymptotic slopes indicate a difference of heterogeneity in the aggregates which only at very large u-values displayed the behavior of linear chains. Evidently, the anomalous angular dependence results from a complex global and segmental structure and aroused interest in a more detailed analysis of these particles as given in a previous paper.[23] In the present paper, we draw conclusions mainly from the global properties. Two further quantities were considered. These are the ratio of the radius of gyration to the hydrodynamic radius $\rho = R_g/R_h$ and the apparent segment density d_{app}.

ρ-Parameter. Further information was obtained from the combination of static and dynamic light scattering data. A structure-sensitive parameter is obtained from the ratio

$$\rho = \frac{R_g}{R_h} \tag{22}$$

The radius of gyration R_g is a geometrically defined parameter and depends on the macromolecular configuration.[39] In contrast,the radius R_h of a hydrodynamically equivalent sphere is, in addition to the geometrical configurations, also determined by hydrodynamic interaction among chain segments.[28] Generally speaking, if two small particles come close together in a laminar flow, the laminar streaming lines start to overlap and cause an attractive force. Therefore, the hydrodynamics strongly depends on the *segment density* in the aggregates. The molar mass dependence of the two radii is largely canceled when their ratio is formed. The ρ-parameter is thus a measure of the deviation of the polymer architecture from a homogeneous impenetrable sphere. A detailed outline is given in ref 28. For the compact sphere structure a value of $\rho = 0.775$ is obtained. For more open conformations (branched macromolecules, coils, or rigid rods) ρ increases, and in the limit of a thin rigid cylinder one has $\rho > 2$. For microgels with many dangling chains at the surface, smaller values in the range of $\rho = 0.35-0.55$ were experimentally found.[40] The ρ-parameter is also affected by the polydispersity[39] of a system and can, therefore, not be regarded as a uniquely related structural parameter for the investigated systems of high polydispersity. Nonetheless, a variation in the ρ-parameter can be used for a qualitative interpretation in terms of local density.

In Table 5 the ρ-values of the PVI samples are listed; the variation of the ρ-parameter with the molar mass is shown in Figure 9. According to the already mentioned findings, for small molar mass PVI macromol-

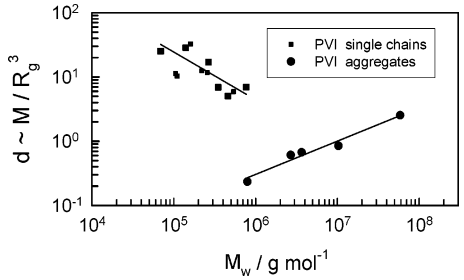

Figure 10. Molar mass dependence of the apparent particle density d_{app}. Opposite changes of d_{app} with the molar mass were observed for the single chains and the aggregated PVI samples.

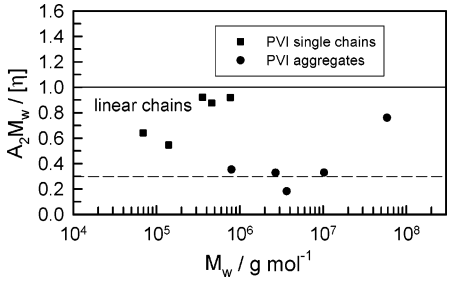

Figure 11. Ratio $A_2M_w/[\eta]$ as a function of the molar mass of molecularly dissolved and aggregated PVI. The solid line represents the asymptotic theoretical curve for linear chains. Fair agreement was obtained with PVI in the low molar mass regime. Much smaller values were found for the aggregates in the high molar mass regime (dotted line) with an average $A_2M_w/[\eta]$ of about 0.30.

ecules a behavior of polydisperse coils in marginal solvent with ρ-values around 1.73 was to be expected. A somewhat lower value of $\rho \cong 1.55$ was experimentally obtained. This could be interpreted that in this M_w regime the macromolecules have a somewhat more contracted structure than predicted by theory. However, recent Brownian motion simulations by Freire et al.[41−43] gave even for a good solvent a ρ-value of about 1.5. This difference from the analytic theory results from a simplifying assumption on the hydrodynamic interaction that was required in the analytic theory.[31,44] A striking dependence was observed for the PVI aggregates. Near $M_w = 8 \times 10^5$ g/mol the ρ-parameter started with a value of 1.87 but then strongly decayed with the molar mass toward a value as small as 0.58. This value for the highest molar mass in the series is in fact indicative of a micellar structure or microgels with dangling chains as was demonstrated with samples which were cross-linked in uniform latex particles. The soap was removed, and the resulting swollen microgels were measured by static and dynamic light scattering in an organic solvent.[40] Thus, the aggregates resemble microgels in which the chains are not chemically linked together but kept bound by physical forces or bonds.

Apparent Density. The highly contracted structure of the particles with $M_w > 8 \times 10^5$ g/mol was confirmed by the variation of the apparent particle density with the molar particle mass (Figure 10). This density was calculated on the basis of a smeared uniform density in the particle and is based on eq 23 for equivalent

$$d_{app} = \frac{M_w}{N_A(4\pi/3)R_g^3} \tag{23}$$

homogeneous spheres. Again two domains were observed with a negative slope for the single chains, a positive slope for the aggregstes, and a variation by a factor of 20 around the break point of $M_w \approx 8 \times 10^5$ g/mol. The negative slope is in agreement with the common behavior of flexible chains, but the positive slope is characteristic of increasing packing in aggregates.

Finally, we show in Figure 11 the ratio $Y = A_2M_w/[\eta]$ as a function of M_w for PVI in the two molar mass regimes. Both quantities in the numerator and the denominator are proportional to R_g^3/M, which cancel in the ratio. What is left is the ratio Ψ/Φ in which Ψ is the coil−coil interpenetration factor and Φ Flory's draining function. In other words the ratio compares the coil−coil interaction with the hydrodynamic interaction among the particles. Also this parameter displays a drastic difference in behavior in the two molar mass regimes. For linear flexible chains the value of the ratio is close to the theoretical value of $Y = 1.04$.[45] For star-branched chains the Y-ratio value increases with the number of arms[46] and reaches a limit at about $Y = 2.2 \pm 0.2$ for high molar mass.[47−49] The value of about $Y = 0.30$ found for the present aggregates demonstrates the remarkable difference from randomly branched materials.

Break in Behavior. The stunning and strikingly abnormal break in the solution properties may now be commented on. At present we have no special experimental data in our hands which conclusively would explain *why* such a break in behavior could occur. We measured infrared spectra from samples of low molar mass and from the aggregates, and recorded the spectra from powders and films. The spectra showed no differences. There are, however, other observations and facts which in our view remain worth considering.

Commonly, free radical polymerization is made with polymers which are soluble in the monomer liquid or at least soluble in a suitable solvent. This means that the polymer remained in a coil conformation before it was precipitated for further purification. In these cases soluble samples of increasingly longer chains can be prepared by reducing the initiator concentration or lowering the reaction temperature. This is the most observed behavior. Another situation is encountered when the polymer is not fully soluble in the monomer or the required solvent. With increasing extent of monomer conversion but also with increasing chain length partial precipitation occurs and mostly a gel-like precipitant is obtained. This case was extensively treated by Bamford et al.[50] The authors considered diffusion-controlled termination and occlusion of polymer radicals in a collapsed particle. A considerable deviation from the common Schulz−Flory most probable distribution was deduced. An essentially different situation is present with the precipitating polymerization of vinylimidazole. The polymer is not or is only poorly soluble in the monomer, and also it is insoluble in toluene or benzene. The precipitation is very efficient such that almost no swelling and no gel formation occurred. The precipitated polymer included almost no benzene or toluene and was quickly transformed into the glassy state. (Actually this is the main advantage of this recipe of vinylimidazole polymerization; the precipitant could be easily washed in toluene or benzene, whereas in other solvents a sticky material is obtained that is difficult to purify.)

A significant influence on the kinetics could be expected as a consequence of the sharp transition into

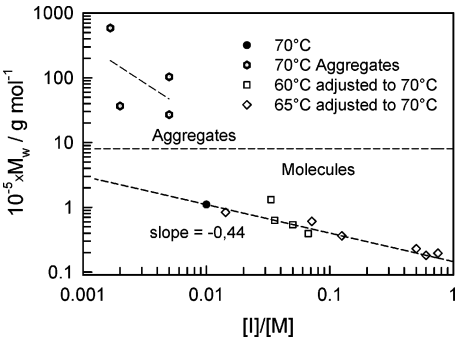

Figure 12. Molar mass dependence of the molecularly dissolved PVI from the molar initiator/monomer ratio [I]/[M] in the precipitating radical polymerization in benzene or toluene at 70 °C. Measurements at 65 and 60 °C were adjusted to the reference temperature of 70 °C. The horizontal dashed line indicates the molar mass when we observed aggregate formation. The transition to aggregate formation occurred in the range of $0.005 < [I]/[M] < 0.01$ at 70 °C.

the glassy state. Surprisingly, this seems not to be the case with our samples. We checked how the chain length was increased when the initiator/monomer ratio in benzene or toluene was reduced. These two solvents are known to have the lowest chain transfer in radical polymerization and can be considered as an inert dilution reagent. Under the neglect of chain transfer the chain length is predicted to increase propertional to $([I]/[M])^{-0.5}$. In Figure 12 we plotted the molar mass against [I]/[M] on a double-logarithmic scale and found an exponent of -0.44, close to the theoretically expected value of -0.5. The somewhat lower value may arise from the polydispersity, because the kinetics requires the number-average molar mass. The curve gave no indication of a failure in the kinetics of preparing high molecularly dissolved chain molecules. Evidently, the quite normal kinetics cannot be responsible for the aggregate formation, and another reason has to be found. No direct comparison with the literature for the kinetics of PVI could be made because corresponding measurements were carried out in DM,[51] which is a poor solvent for PVI, and not in the sharply precipitating toluene.

The main difference in the PVI precipitation by toluene or benzene from common precipitation is that a liquid/solid phase separation and not the common and well-understood liquid/liquid phase separation is effective. The only explanation for the unexpected transition to aggregates, we can think of, is that domains in the glassy material become stabilized once a certain chain length is exceeded. On dissolution in ethanol these stabilized domains apparently remained in a metastable state. The determination of reliable liquid/solid-state phase diagrams is known to be difficult, because often the phase temperature on cooling is lower than obtained on heating, where the precipitate becomes soluble. Apparently, the measured curves do not represent thermodynamic equilibrium states.

The kinetic curve of Figure 12 makes it clear that the break point actually is not simply a point, but represents at least a transition region; probably the two curves in Figure 12 even partially overlap. Fractionation of samples slightly below the break point may well lead to high molar masses which show no aggregations, because the material was all the time in the molecularly dispersed state. In addition one has to keep in mind that the PVIA is actually a sol fraction from the gel that was obtained at a very low initiator/monomer ratio, which explains the fairly low molar mass of an aggregate. Aggregates are mostly stabilized by noncovalent forces which increase with the number of contacts and thus with the chain length of polymeric unimers. These forces, common in many biopolymers, lead to incomplete dissolution. The dissolution will stop when the particles become sterically stabilized.[52] Complete dissolution will occur when the chain length is sufficiently short such that the solvation power of the solvent can break up the structure. A certain overlap was observed with the same samples dissolved in 0.5 M $NaNO_3$ aqueous solutions.[53]

The question of what type of forces may be active in the aggregates remains open. With our data of the global structure we cannot answer this question, but some observations from the literature may give a hint. Overberger and Vorchheimer[24,25] pointed out that the water cannot be completely removed from the monomer and polymer at temperature below 100 °C, which means that the water must be tightly bound to the imidazole ring. In fact, elemental analysis gave an indication of tightly bound water that was not removed after freeze-drying and additional drying in an exsiccator. The water content ranged from 0.3 to 0.7 mol of water per monomeric repeat unit, which are exactly the same data as reported by Overger et al.[24.25]

Conclusions

The results from the so-called global quantities revealed a marked transition in behavior around a molar mass of $M_w \approx 8 \times 10^5$ g/mol that appeared like a break. In the low molar mass regime common behavior of molecularly dissolved flexible linear chains was observed. Above the break point aggregates were found, which was concluded from the following list of observations: (1) The radii of gyration and hydrodynamic radii strongly *increased* near the break but showed only a weak further increase with the particle molar mass. (2) On the contrary, the second virial coefficient and the intrinsic viscosity *decreased* at the same break point and increased then with a different exponent as observed below the break point. (3) The $\rho = R_g/R_h$ parameter showed in the low molar mass regime the common behavior of flexible chains. Above the break point a drastic decrease was registered to a point that was observed from synthesized microgels. (4) The apparent segment density decreased in the common manner with the molar mass for the samples in the low molar mass regime. On the contrary, the density first sharply decreased slightly above the break point, but then strongly *increased* with growing particle mass.

The shift to smaller values of the second virial coefficient and the intrinsic viscosity and the decrease of the ρ-parameter consistently indicate a change from linear coil toward globular structures. The segments are more densely packed with increasing particle mass. The much larger radii of gyration than the corresponding ones from linear PVI of the same molar mass indicate segment packing in the aggregates that is correlated to a stiffening of the objects. These stiff elements could be recognized in AFM micrographs.

The key point in our conclusion is that we have to keep in mind the dissolution mechanism, and not how such structures are formed from solution via association. Aggregates are metastable objects and have to be distinguished from associated structures. The latter is in thermodynamic equilibrium, the former not.

Supporting Information Available: Results of elemental analysis and FTIR spectra from PVI fraction VII as examples of low M_w samples (forming a molecularly dispersed solution) and PVIB from the aggregate-forming group. This material is available free of charge via the Internet at http://pub.acs.org.

References and Notes

(1) Gold, H. D.; Gregory, H. P. *Z. Phys. Chem. Neue Folge* **1958**, *15*, 93.
(2) Liu, K. J.; Gregor, H. P. *J. Phys. Chem.* **1965**, *69*, 1248.
(3) Henrichs, P. M.; Whitlock, L. R.; Sochor, A. R.; Tan, J. S. *Macromolecules* **1980**, *13*, 1375.
(4) Kodama, H.; Miyajima, T.; Mori, M.; Takahashi, M.; Nishimura, H.; Ishiguro, S. *Colloid Polym. Sci.* **1997**, *275*, 938. Kodama, H.; Miyajima, T.; Tabuchi, H.; Ishiguro, S. *Colloid Polym. Sci.* **2000**, *278*, 1.
(5) Liu, K. J.; Gregor, H. P. *J. Phys. Chem.* **1965**, *69*, 1248.
(6) Lippert, J. L.; Robertson, J. A.; Havens, J. R.; Tan, J. S. *Macromolecules* **1985**, *18*, 63.
(7) Gold, D. H.; Gregor, H. P. *J. Phys. Chem.* **1960**, *64*, 1464.
(8) Liu, K. J.; Gregor, H. P. *J. Phys. Chem.* **1965**, *69*, 1252.
(9) Sato, M.; Kondo, K.; Takemoto, K. *Makromol. Chem.* **1978**, *179*, 601.
(10) Sato, M.; Kondo, K.; Takemoto, K. *Makromol. Chem.* **1979**, *180*, 699.
(11) Suzuki, M.; Kobayashi, S.; Uchida, S.; Kimura, M.; Hanabusa, K.; Shirai, H. *Macromol. Chem. Phys.* **1998**, *199*, 937.
(12) Suzuki, M.; Yokoyama, N.; Kimura, M.; Hanabusa, K.; Shirai, H. *Macromol. Chem. Phys.* **1998**, *199*, 2267.
(13) Pekel, N.; Güven, O. *Colloid Polym. Sci.* **1999**, *277*, 570.
(14) Luo, X.; Goh, S. H.; Lee, S. Y. *Macromol. Chem. Phys.* **1999**, *200*, 399.
(15) Luo, X.; Goh, S. H.; Lee, S. Y.; Huan, C. H. A. *Macromol. Chem. Phys.* **1999**, *200*, 874.
(16) Letsinger, R. L.; Klaus, I. S. *J. Am. Chem. Soc.* **1965**, *87*, 3380.
(17) Grampel, H. T.; Tan, Y. Y.; Challa, G. *Macromolecules*, **1992**, *25*, 1041.
(18) Roques-Carmes, T.; Membrey, F.; Filiatre, C.; Foissy, A. *J. Colloid Interface Sci.* **2002**, *245*, 257.
(19) Hansen, J.; Kumagai, M.; Ishida, H. *Polymer* **1994**, *35*, 4780.
(20) Kumagai, M.; Tsuchchida, K.; Ogino, Y.; Hansen, J.; Ishida, H. *Polymer* **1995**, *36*, 535.
(21) Molina, M. J.; Morales, E.; La Mantia, F. P. *Polym. Networks Blends* **1995**, *5*, 141.
(22) Tan, J. S.; Sochor, A. R. *Macromolecules* **1981**, *14*, 1700.
(23) Savin, G.; Burchard, W. *Macromolecules*, in press.
(24) Overberger, C. G.; Vorchheimer, N. *J. Am. Chem. Soc.* **1963**, *85*, 951.
(25) Overberger, C. G.; Vorchheimer, N.; Yaraslavsky, S. *J. Am. Chem. Soc.* **1965**, *87*, 296.
(26) For details see textbooks on polymer science and monographs on light scattering, e.g. (a) Huglin, M. B. *Light Scattering from Polymer Solutions*; Academic Press: London, 1972. (b) McIntyre, D., Gornick, F., Eds. *Light Scattering from Dilute Polymer Solutions*; Gordon and Breach: New York, 1964. (c) Burchard, W. Light Scattering Techniques. In *Physical Techniques for the Study of Food Biopolymers*; Ross-Murphy, S. B., Ed.; Blackie Academic & Professional: London, 1974.
(27) Zimm, B. H. *J. Chem. Phys.* **1948**, *16*, 1099.
(28) Burchard, W. *Adv. Polym. Sci.* **1999**, *143*, 113.
(29) Guinier, A. *Ann. Phys.* **1939**, *12*, 161. (b) Guinier, A.; Fournet, G. *Small Angle Scattering of X-Rays*; Wiley & Sons: New York, 1955.
(30) For details see: Berne, B. J.; Pecora, R. *Dynamic Light Scattering*; Wiley & Sons: New York, 1976.
(31) Yamakawa, H. *Modern Theory of Polymer Solutions*; Harper & Row: New York, 1971.
(32) Freed, K. F. *Renormalization Theory of Macromolecules*; Wiley & Sons: New York, 1987.
(33) Stanley, H. E. *Introduction to Phase Transitions and Critical Phenomena*; Oxford University Press: Oxford, 1971; Chapter 11.
(34) Stauffer, D. *Introduction to Percolation Theory*; Taylor & Francis: London, 1985.
(35) Daoud, M.; Martin, J. E. Fractal Properties of Polymers. In *The Fractal Approach to Heterogeneous Chemistry*; Avnir, D., Ed.; Wiley & Sons: New York, 1989.
(36) De Gennes, P. G. *Scaling Concepts in Polymer Physics*; Cornell University Press: Ithaca, NY, 1979.
(37) Burchard, W.; Kajiwara, K.; Nerger, D. J. *Polym. Sci., Phys. Ed.* **1982**, *20*, 157.
(38) Dozier, W. D.; Huang, J. S.; Fetters, L. J. *Macromolecules* **1991**, *24*, 2810.
(39) Burchard, W.; Schmidt, M.; Stockmayer, W. H. *Macromolecules* **1980**, *13*, 1265.
(40) (a) Burchard, W.; Schmidt, M. *Ber. Bunsen-Ges. Phys. Chem.* **1979**, *83*, 388. (b) Schmidt, M.; Nerger, D.; Burchard, W. *Polymer* **1979**, *20*, 582.
(41) Freire, J. J.; Pla, J.; Rey, A.; Prats, R. *Macromolecules* **1986**, *19*, 452.
(42) Freire, J. J.; Rey, A.; Garcia de la Torre, J. *Macromolecules* **1986**, *19*, 457.
(43) Rey, A.; Freire, J. J.; Garcia de la Torre, J. *Macromolecules* **1987**, *20*, 342.
(44) Kirkwood, J. G.; Riseman, J. *J. Chem. Phys.* **1948**, *16*, 565.
(45) (a) Reference 32, p 238. (b) Huber, K. Burchard, W.; Akcasu, Z. A. *Macromolecules* **1985**, *18*, 2743.
(46) (a) Roovers, J.; Zhou, L. L.; Toporowski, P. M.; van der Zwan, M.; Iatrou, H.; Hadjichristidis, N.*Macromolecules* **1993**, *26*, 4324. (b) Bywater, S. *Adv. Polym. Sci.* **1979** *30*, 89. (c) Roovers. J.; Bywater, S. *Macromolecules* **1972**, *5*, 384; **1974**, *7*, 443.
(47) Bauer, J.; Burchard, W. *Macromolecules* **1993**, *26*, 3103.
(48) Galinsky, G.; Burchard, W. *Macromolecules* **1996**, *29*, 1498.
(49) Reference 28, pp 173−175.
(50) Bamford, C. H.; Barb, W. G.; Jenkins, A- D-; Onyon, P. F. *The Kinetics of Vinyl Polymerization by Radical Polymerization*; Butterworth: London, 1958.
(51) Bamford, C. H.; Schofield, E. *Polymer* **1981**, *232*, 1227.
(52) See for instance: Evans, D. F.; Wennerström, H. *The Colloid Domain*; Wiley-VCH Publishers: New York−Weimheim−Cambridge, 1994.
(53) Savin, G.; Burchard, W. Manuscript in preparation.

MA035362G